http://dx.doi.org/10.5012/bkcs.2012.33.5.1541

Nucleation and Growth of Bismuth Electrodeposition from Alkaline Electrolyte

Longping Zhou, Yatang Dai,* Huan Zhang, Yurong Jia, Jie Zhang, and Changxiong Li

School of Materials Science and Engineering, Southwest University of Science and Technology, Mianyang 621010, China
**E-mail: daiyt2003@163.com*
Received January 13, 2012, Accepted February 3, 2012

The early stages of bismuth (Bi) electrodeposition on glass carbon electrode from alkaline electrolyte were studied by cyclic voltammetry, chronoamperometry, scanning electron microscopy, atomic force microscopy and X-ray diffraction. The CV analysis showed that the electrodeposition of Bi was determined to be quasi-reversible process with diffusion controlled. The current transients for Bi electrodeposition were analyzed according to the Scharifker-Hills model and the Heerman-Tarallo model. It can be concluded that the nucleation and growth mechanism was carried out under a 3D instantaneous nucleation, which was confirmed by SEM analysis. The kinetic growth parameters were obtained through a nonlinear fitting. In addition, the Bi film obtaining at −0.86 V for 1 hour was of compact and uniform surface with good smoothness, small roughness and a very high purity. The Bi film were indexed to rhombohedral crystal structure with preferred orientation of (0 1 2) planes to growth.

Key Words : Bismuth, Electrodeposition, Alkaline electrolyte, Nucleation

Introduction

Bismuth (Bi) is a semimetal with a rhombohedral structure. Bi has been attracted many interests from physicists and chemists because of its unique physical and chemical properties. Owing to its large magnetoresistance,[1-5] thermoelectric efficiency[6] and interesting quantum effects,[7] Bi films possessed many applications in electrochromic devices, environmental detection, catalysis, superconductivity, thermoelectric, and piezoelectric.[8-13]

In recent years, electrodeposition is the least expensive, effective, and readily adoptable method to deposit Bi films. Much of previous studies of the electrodeposition of Bi films from nitrate, perchlorate, lactate, silicate, sulfate and pyrophosphate electrolytes.[14-19] Highly textured Bi films with 1 to 15 μm thick have been electrodeposited onto semiconductor substrates,[20,21] noble metals (such as evaporated Au and polycrystalline Cu)[14,22] and glassy carbon electrode.[15] The electrodeposits of Bi have exhibited various morphologies,[22] such as prickly rod, branch, skeleton and strip-like shape.

However, those studies mainly focused on acid electrolyte. But almost all acid electrolytes contain a large excess of free acid which are harmful to both human health and the environment. The Bi films usually are of poor quality because there are hydrogen evolution reactions in acid electrolyte. There is a paucity of studying electrodeposition of Bi films from alkaline electrolyte. The investigation on the initial stage of Bi electrodeposition in alkaline electrolyte, including the nucleus formation and its growth mechanism, is very insufficient. Consequently, an intensive understanding of nucleation and growth during Bi electrodeposition is very important for obtaining Bi films with good quality.

Herein, we reported the electrodeposition of Bi onto glassy carbon electrode (GCE) from alkaline electrolyte, and its nucleation and growth mechanism was investigated. Cyclic voltammetry (CV) and chronoamperometry (CA) techniques were used to study the initial stages of Bi electrodeposition on GCE. The Scharifker-Hills model was used to determine the nucleation and growth mechanism. The Heerman-Tarallo model was used to extract the kinetic parameters of the electrodeposition progress. Scanning electron microscopy (SEM), atomic force microscopy (AFM) and X-ray diffraction (XRD) were used to determine the surface morphologies and crystal structure of Bi electrodeposits.

Experimental

The Bi electrodeposition electrolyte consists of 80 g L^{-1} $Bi(NO_3)_3$, 90 g L^{-1} ethylene diamine tetraacetic acid (EDTA), 120 g L^{-1} 5-sulfosalicylic acid, 75 g L^{-1} potassium sodium tartrate and 80 g L^{-1} KCl. The pH of the electrolyte was adjusted to 8-9 by adding drops of high concentrated KOH (500 g L^{-1}). All the chemicals used in this work were analytical grade. Electrochemical measurements were performed at Pine AFCBP1 Bipotentiostat (Pine Instrument Company, USA). The electrochemical experiments, including CV and CA measurements, were carried out in a three-electrode cell configuration with a GCE (3 mm in diameter) as working electrode, a saturated calomel electrode (SCE) as reference electrode and platinum wire as counter electrode. All potentials were given *versus* the SCE electrode.

Prior to the electrochemical experiments, GCE was mechanically polished to a mirror-like with slurry of alumina, and then cleaned in an ultrasonic bath of distilled water for 2 min. CV measurements were performed in the potential range between +400 and −900 mV at different scan rates.

CA measurements were carried out by using a cathodic pulse from 0 mV to different deposition potentials from −770 mV to −890 mV. In order to clear out the residual metal, GCE were cleaned by continuously sweeping at +500 mV for 1 min before each experiment. The surface morphologies and crystal structures of Bi electrodeposits were examined by S440 stereo SEM (Leica Microsystems Cambridge Ltd Company, UK) operating at 25 kV and 200 pA, SPI3800N AFM (SIINT Company, Japan), and X' Pert PRO XRD (Panalytical Company, Netherland) operating at 35 kV and 60 mA with Cu Kα radiation.

Results and Discussion

Cyclic Voltammetry. CV was used to define the potential region for deposition and dissolution of Bi on GCE. Figure 1 shows a series of cyclic voltammograms for Bi electrodeposition on GCE from alkaline electrolyte at different scan rates. The cyclic voltammograms were consistent with that of typically observed in metal deposition-stripping processes. Each curve displays a couple of well-defined cathodic and anodic peaks and a crossover between the cathodic and anodic branches. The presence of the crossover of the reverse anodic scan over the cathodic scan, giving rise to what has been called the "nucleation loop",[23] which indicated the formation of Bi nuclei on GCE. Also, it can be seen from Figure 1 that the peak potential shifts to more negative potentials upon increasing the scan rate, which was typically associated with quasi-reversible electrochemical reactions.[14] In order to determine the type of control limiting the deposition process, the cathodic peak current (I_{Peak}) *versus* the square root of the sweep rate ($\nu^{1/2}$) for the cyclic voltammograms was plotted and shown in Figure 2. It can be seen that the plot displays an excellent linear relationship, indicating a diffusion controlled process.

Nucleation and Growth Mechanism. The study of nucleation and growth via electrochemical methods offers a certain advantage over other methods, because the driving force of nucleation can be simply varied by changing the applied potential. Therefore, the mechanism of nucleation

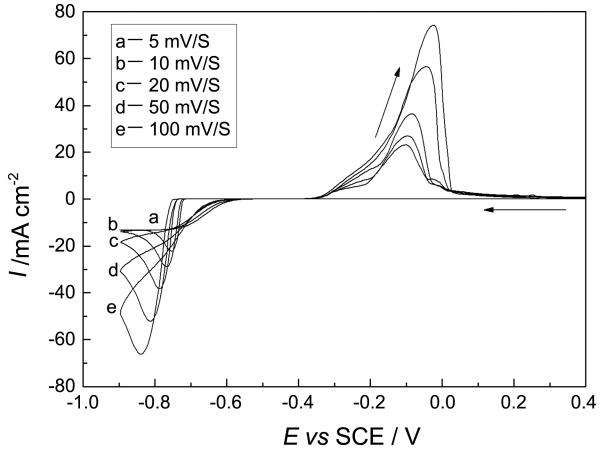

Figure 1. Cyclic voltammograms for Bi electrodeposition on GCE from alkaline electrolyte at different scan rates.

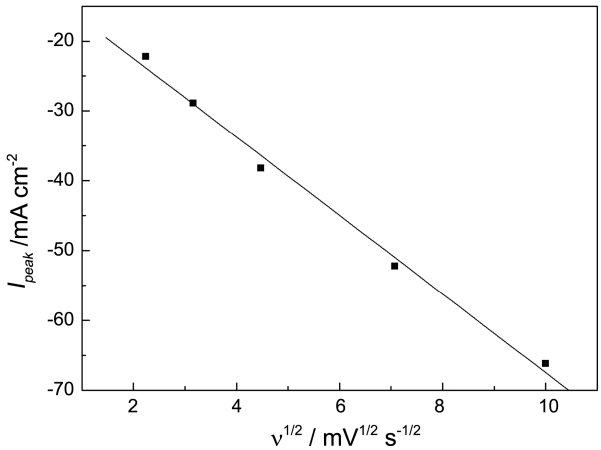

Figure 2. Plot of the cathodic peak current (I_{Peak}) *versus* the square root of the sweep rate ($\nu^{1/2}$) for the cyclic voltammograms presented in Figure 1.

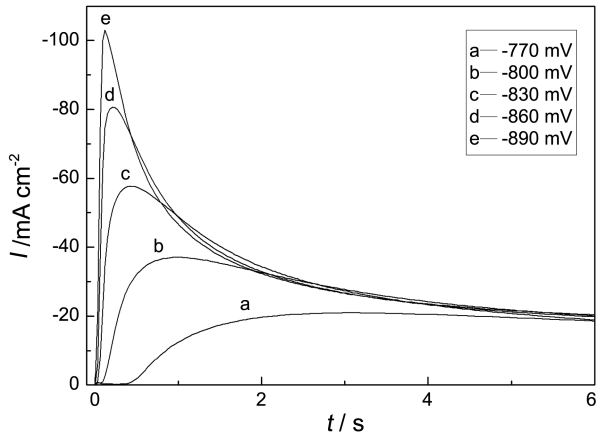

Figure 3. Current transients for Bi electrodeposition on GCE from alkaline electrolyte at different deposition potentials. The starting potential was 0 V.

and growth can be determined by analysis of current transients from CA measurements. Figure 3 shows a series of current transients for Bi electrodeposition on GCE from alkaline electrolyte at different deposition potentials. After applying the potential step, due to the double layer charging, a rise and then fall in current can be observed, which is characteristic of Bi nucleation and growth.[14,15,24] In this latter region, the current maximum (I_{max}) increases while the time (t_{max}) required to reach I_{max} decreases with increasing overpotential as a consequence of the higher nucleation densities.[14] Figure 4 shows a series of current transients (I) *versus* $t^{-1/2}$ curves for CA measured value presented in Figure 3. It can be seen that the current transients in the last part showed a good linear relationship according to the Conttrell equation. And these curves present a function of $t^{-1/2}$ relaxation as individual hemispherical diffusion zones overlap to form a linear diffusion gradient,[25] which is a typical response of three-dimensional (3D) multiple nucleation with diffusion controlled growth.[26,27]

The 3D-nucleation model with hemispherical diffusion control to the growing 3D clusters describes the kinetics of

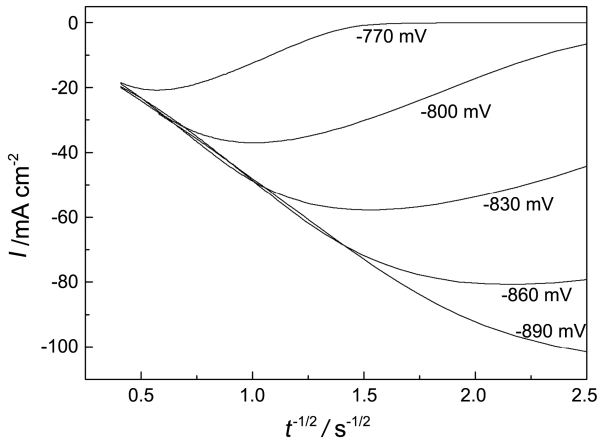

Figure 4. Current transients (I) *versus* $t^{-1/2}$ curves for CA measured value presented in Figure 3.

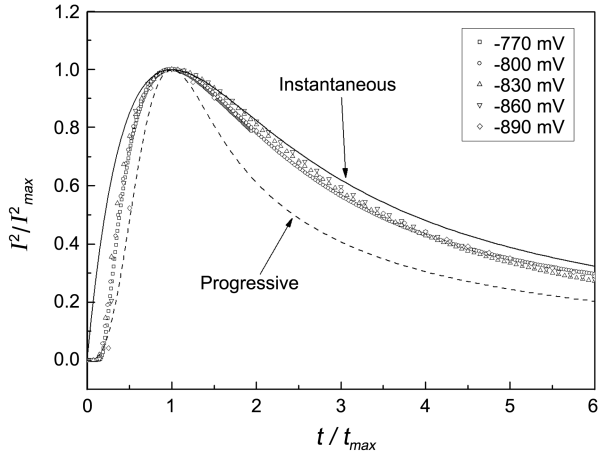

Figure 5. Comparison of theoretical non-dimensional $(I/I_{max})^2$ *vs.* t/t_{max} plots for instantaneous nucleation from Eq. (1) and progressive nucleation from Eq. (2), to the experimental current transients of Figure 3.

electrolytic phase formation at the early stages, when diffusion of the depositing species from the bulk of the solution to the electrode/solution interface is the slow step of the process, considering the eventual overlap of diffusion zones and the development of nucleation exclusion zones around already established nuclei.[28,29] Scharifker-Hills[25] have developed a convenient model to identify the nucleation and growth mechanism. According to this model, there are two limiting nucleation and growth mechanisms, *i.e.* the instantaneous and progressive nucleation. For instantaneous nucleation, all nuclei are immediately formed after it is applied a potential step. While in progressive nucleation, the number of nuclei increases gradually with the deposition time.[30]

The expressions for instantaneous and progressive nucleation with 3D growth are given by Eq. (1) and Eq. (2), respectively.[25]

$$\left(\frac{I}{I_{max}}\right)^2 = 1.9542\left(\frac{t}{t_{max}}\right)^{-1}\left\{1-\exp\left[-1.2564\left(\frac{t}{t_{max}}\right)\right]\right\}^2 \quad (1)$$

$$\left(\frac{I}{I_{max}}\right)^2 = 1.2254\left(\frac{t}{t_{max}}\right)^{-1}\left\{1-\exp\left[-2.3367\left(\frac{t}{t_{max}}\right)^2\right]\right\}^2 \quad (2)$$

Where I_{max} is the maximum current density, and t_{max} is the time corresponding to the maximum current density. Eq. (1) and (2) provide a convenient criterion for distinguishing between these two extreme cases of nucleation kinetics. The experimental data may be presented in a nondimensional plot, $(I/I_{max})^2$ *vs.* t/t_{max}, facilitating comparison with the behavior predicted for each of these limiting nucleation and growth mechanisms.[30]

Figure 5 shows a non-dimensional plot of the experimental current transients for Bi electrodeposition onto GCE from alkaline electrolyte at different deposition potentials. The figure shows that at a very short time, before reaching the maximum points, all of the experimental curves change from the 3D progressive nucleation toward 3D instantaneous nucleation. After for longer periods, during the fall of the current transients, the experimental curves were a little negative deviation from the 3D instantaneous nucleation. Thus, it appears that nucleation and growth mechanism was carried out under a 3D instantaneous nucleation. Similar results can be also found in several papers by other authors.[15,29]

In order to extract quantitative information on the kinetics mechanism associated with the Bi nucleation and growth process, the model of Heerman-Tarallo[31] have proposed a convenient method to identify the typical kinetics parameters. According to this model, which merges the approaches of Sharifker-Mostany[32] and Sluyter-Rehbach,[33] the nucleation rate constant (A), and the number density of active sites (N_0) can be fitting the entire experimental current density transients to the following expression[31]:

$$I(t) = zFDC(\pi DT)^{-1/2}\frac{\Phi}{\Theta}\{1-\exp[-\alpha N_0(\pi DT)^{1/2}t^{1/2}\Theta]\}, \quad (3)$$

with

$$\Phi = 1-\frac{\exp(-At)}{(At)^{1/2}}\int_0^{(At)^{1/2}}\exp(\lambda^2)d\lambda \quad (4)$$

$$\Theta = 1-\frac{1-\exp(-At)}{At} \quad (5)$$

$$\alpha = 2\pi(2MDC/\rho)^{1/2}. \quad (6)$$

Where zF (z is the number of electron involved in the chemical reaction and F is the Faraday's constant) is the molar charge transferred during electrodeposition, D is the diffusion coefficient, C is the metal ion bulk concentration, M is the molar mass and ρ is the density of the Bi deposit. The function Φ is directly related to the Dawson's integral and reflects the retardation of the current by slow nucleation, and Θ reflects the retardation of the growth of the coverage as a result of slow nucleation.[28] The Eq. (3) has some mathematical complexity due to the presence of Dawson's integral in calculate the kinetics parameters. Since the function $F(x)=\exp(-x^2)\int_0^x \exp(\lambda^2)d\lambda$ can be efficiently approximated with the polynomial[34]

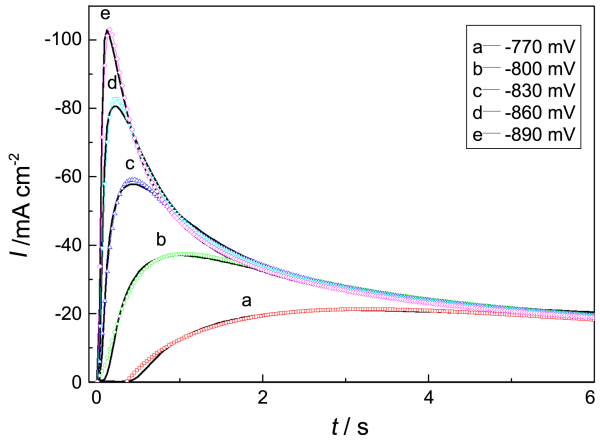

Figure 6. Comparison between the experimental current transients (solid line) and the corresponding theoretical current transients (dot line) obtained by nonlinear fitting the Eq. (3) to the experimental data.

$$F(x) = \frac{0.051314213 + 0.47910725x}{1 - 1.2068142x + 1.185724x^2}. \quad (7)$$

Eq. (4) can be rewritten as

$$\Phi = \frac{0.52089275 - 1.2068142A^{1/2}t^{1/2} + 1.185724At - 0.051314213A^{-1/2}t^{-1/2}}{1 - 1.2068142A^{1/2}t^{1/2} + 1.185724At}. \quad (8)$$

1stOpt (7D-Soft High Technology Inc., China) as a commercial software based on the Levenberg-Marquardt algorithm was served as the tool for the nonlinear fitting. Figure 6 shows a comparison between the experimental current transients and the corresponding theoretical current transients obtained by nonlinear fitting the Eq. (3) to the experimental data using A, N_0 and D as fitting parameters. The constants of the nonlinear fitting were: zF = 289456 C mol^{-1}, C = 1.6491 × 10^{-4} mol cm^{-3}, M = 208.98 g mol^{-1} and ρ = 9.8 g cm^{-3}. As it is showed in Figure 6, the Heerman-Tarallo model could be applied with sufficient accuracy in the studied potential range and the best-fit of these kinetics parameters, A, N_0 and D, were listed in Table 1. It can be concluded that A were linear growth and N_0 were exponential growth with the increase of deposition potential, while D (3.0 ± 0.14 × 10^{-6} cm^2 s^{-1}) almost unchanged. Similar results can be also found in several papers by other authors.[28-30] The behaviour of N_0 indicates the existences of energies distribution on the surface with a larger fraction of sites are becoming active with the increase of deposition potential.[35] If the influence of hydrogen evolution reaction is lesser, with the increase of N_0 values, it is easier to get less crystal sizes, more compact structure and better performance of Bi films.

Table 1. Kinetic parameters of the Bi electrodeposition on GCE from alkaline electrolyte

E *vs* SCE (V)	A (s^{-1})	N_0 (× 10^6 cm^{-2})	D (× 10^{-6} cm^2 s^{-1})
−0.77	1.06	0.27	2.86
−0.80	4.57	0.57	3.03
−0.83	10.66	1.42	3.04
−0.86	16.52	2.95	2.99
−0.89	22.99	4.96	2.88

Characterization. Figure 7 shows the SEM micrographs of Bi electrodeposits on GCEs from alkaline electrolyte at different deposition potentials for CA experiments. Figure 7(a) corresponds to the Bi electrodeposits at −0.80 V for 10s. It can be seen from Figure 7(a) that the polygonal crystals were randomly distributed over the surface, with particle sizes of 0.8-1.6 μm. Figure 7(b) corresponds to the Bi electrodeposits at −0.86 V for 10s. In Figure 7(b) the irregular crystals were densely and randomly distributed over the surface, with particle sizes of 0.1-0.4 μm. These results indicated that the Bi electrodeposits showed 3D morphological characteristics. As the deposition potential increased, the number density of nuclei turned denser and the particle sizes became smaller. This observation is in good agreement with the results obtained from the study of experimental current transients, in which the nucleation rate constants (A)

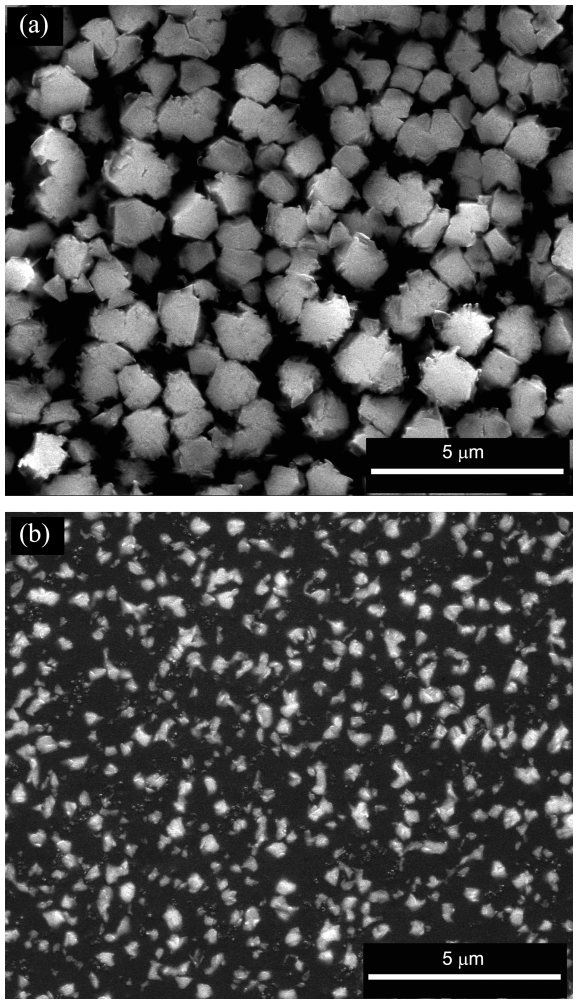

Figure 7. SEM micrographs of Bi electrodeposits obtained on glassy carbon electrodes from alkaline electrolyte at different deposition potentials. (a) At −0.80 V for 10s. (b) At −0.86 V for 10s.

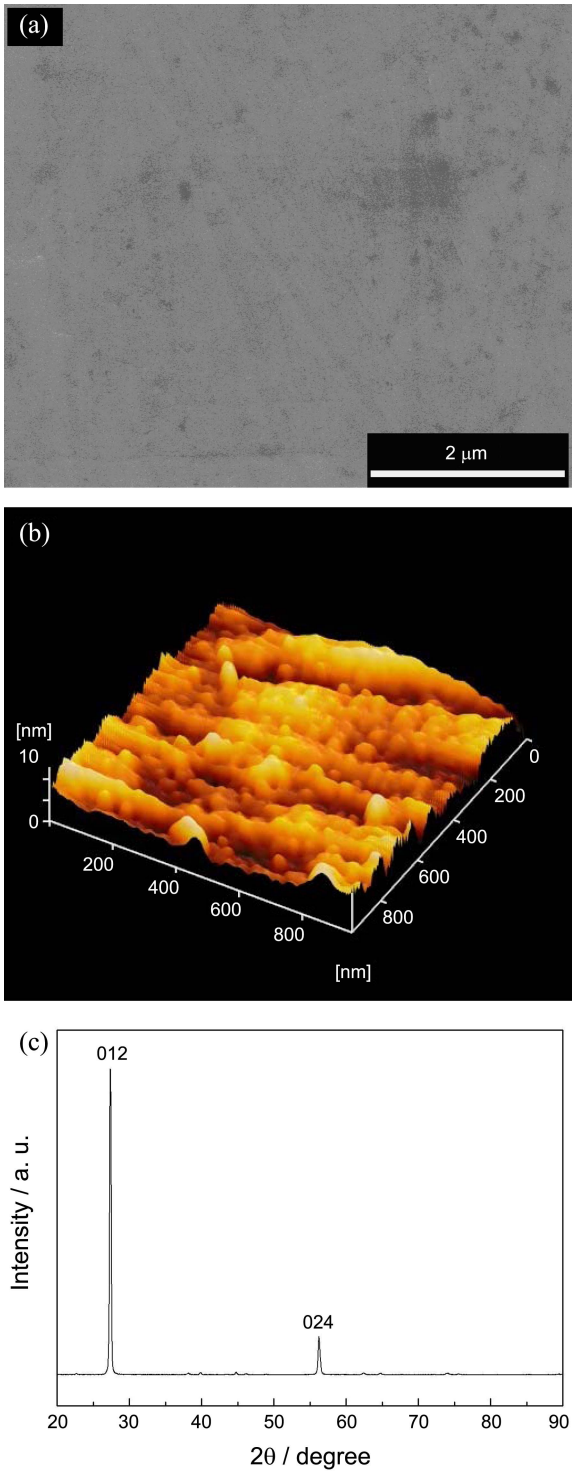

Figure 8. (a) SEM micrograph, (b) AFM image and (c) XRD pattern of Bi film obtained on glassy carbon electrode from alkaline electrolyte at −0.86 V for 1 hour.

are linear growth and the number density of active sites (N_0) are exponential growth with the increase of deposition potential. This is suggested that the morphologies of Bi electrodeposits can be adjusted by controlling the deposition potential.

Figure 8 shows the morphology and crystal structure of Bi film obtained on glassy carbon electrode from alkaline electrolyte at −0.86 V for 1 hour. It can be seen from Figure 8(a) that the Bi film was of compact and uniform surface with good smoothness. As seen from the AFM image of Bi film (Fig. 8(b)), the average surface roughness (*R*a), the root-mean-squared surface roughness (*R*rms) and the maximum Peak-to-valley distance ($R_{P\text{-}V}$) of the Bi film were 1.239 nm, 1.535 nm and 12.77 nm, respectively. It can be concluded that the surface of the Bi film was of small roughness and good smoothness. Figure 8(c) corresponds to the XRD pattern of the Bi film. In this figure, Bi film has a rhombohedral crystal structure (space group *R*-3m) with lattice parameters a = 0.455 nm, b = 0.455 nm and c = 1.186 nm. To Bi film, the purity was very high, and it was preferred orientation of (0 1 2) and (0 2 4) planes to growth. A similar result was also being reported in other studies of Bi electrodeposition film.[14] The results of the SEM micrograph, the AFM image and the XRD pattern analysis of the Bi film indicated that the Bi film was of compact and uniform surface with good smoothness, small roughness and a very high purity.

Conclusions

In this paper the very initial stages of the Bi electrodeposition process on GCE from alkaline electrolyte were studied by CV and CA, and it indicated that the nucleation and growth of Bi electrodeposition was carried out under a 3D instantaneous nucleation with diffusion controlled. A comparison between the experimental current transients and the corresponding theoretical current transients obtained by nonlinear fitting the Heerman-Tarallo equation to the experimental data showed that the Heerman-Tarallo model could be applied with sufficient accuracy in the studied potential range. The quantitative analysis of the experimental current transients by Heerman-Tarallo model showed that A were linear growth and N_0 were exponential growth with the increase of deposition potential, while D were almost unchanged.

The SEM micrographs analysis of the Bi electrodeposits showed that the number density of nuclei turned denser and the particle sizes became smaller with the increase of deposition potential, which were consistent with the results obtained from the study of experimental current transients. The Bi film obtaining at −0.86 V for 1 hour was of compact and uniform surface with good smoothness, small roughness and a very high purity. The Bi film has a rhombohedral crystal structure with preferred orientation of (0 1 2) planes to growth.

Acknowledgments. The authors wish to thank the State Key Laboratory Cultivation Base for Nonmetal Composites and Functional Materials for financial and technological support of this work.

References

1. Yang, F. Y.; Strijkers, G. J.; Hong, K.; Reich, D. H.; Searson, P. C.;

Chien, C. L. *J. Appl. Phys.* **2001**, *89*, 7206.
2. Yang, F. Y.; Liu, K.; Chien, C. L.; Searson, P. C. *Phys. Rev. Lett.* **1999**, *82*, 3328.
3. Cho, S.; Kim, Y.; Olafsen, L. J.; Vurgaftman, I.; Freeman, A. J.; Wong, G. K. L.; Meyer, J. R.; Hoffmann, C. A.; Ketterson, J. B. *J. Magn. Magn. Mater.* **2002**, *239*, 201.
4. Jiang, S.; Huang, Y. H.; Luo, F.; Du, N.; Yan, C. H. *Inorg. Chem. Commun.* **2003**, *6*, 781.
5. Tolutis, R. A.; Balevicius, S. *Phys. Status Solidi A* **2006**, *203*, 600.
6. Li, L.; Zhang, Y.; Li, G.; Zhang, L. *Chem. Phys. Lett.* **2003**, *378*, 244.
7. Lu, M.; Zieve, R. J.; van Hulst, A.; Jaeger, H. M.; Rosenbaum, T. F.; Radelaar, S. *Phys. Rev. B* **1996**, *53*, 1609.
8. Ziegler, J. P. *Sol. Energy Mater. Sol. Cells* **1999**, *56*, 477.
9. Torresi, S. I. C.; Carlos, I. A. *J. Electroanal. Chem.* **1996**, *414*, 11.
10. Xiao, F.; Hangarter, C.; Yoo, B.; Rheem, Y.; Lee, K. H.; Myung, N. V. *Electrochim. Acta* **2008**, *53*, 8103.
11. Zhou, B.; Li, X. H.; Zhu, J. J. *Cryst. Growth Des.* **2007**, *7*, 2276.
12. Hutton, E. A.; Ogorevc, B.; Smyth, M. R. *Electroanalysis* **2004**, *16*, 1616.
13. Lee, G. J.; Lee, H. M.; Rhee, C. K. *Electrochem. Commun.* **2007**, *9*, 2514.
14. Sandnes, E.; Williams, M. E.; Bertocci, U.; Vaudin, M. D.; Stafford, G. R. *Electrochim. Acta* **2007**, *52*, 6221.
15. Yang, M.; Hu, Z. *J. Electroanal. Chem.* **2005**, *583*, 46.
16. Perelygin, Yu. P.; Yu. Kireev, S.; Yu. Kireev, A. *Russ. J. Appl. Chem.* **2006**, *79*, 1200.
17. Liu, L.; Wang, L.; Yin, H.; Li, Y.; He, X. *Anal. Lett.* **2006**, *39*, 879.
18. Lu, D.; Wang, J.; Ninivin, C. L.; Mabic, S.; Dimitrakopoulos, T. *J. Electroanal. Chem.* **2011**, *651*, 46.
19. Petrova, T. P.; Zelenetskaya, K. V.; Rakhmatullina, I. F.; Shapnik, M. S. *Prot. Met*. **2006**, *42*, 359.
20. Vereecken, P. M.; Sun, L.; Searson, P. C.; Tanase, M.; Reich, D. H.; Chien, C. L. *J. Appl. Phys.* **2000**, *88*, 6529.
21. Vereecken, P. M.; Searson, P. C. *J. Electrochem. Soc.* **2001**, *148*, 733.
22. Jiang, S.; Huang, Y. H.; Luo, F.; Du, N.; Yan, C. H. *Inorg. Chem, Commun.* **2003**, *6*, 781.
23. Grujicic, D.; Pesic, B. *Electrochim. Acta* **2002**, *47*, 2901.
24. Lai, Y.; Liu, F.; Li, J.; Zhang, Z.; Liu, Y. *J. Electroanal. Chem.* **2010**, *639*, 187.
25. Scharifker, B.; Hills, G. *Electrochim. Acta* **1983**, *28*, 879.
26. Mostany, J.; Mozota, J.; Scharifker, B. R. *J. Electroanal. Chem.* **1984**, *177*, 25.
27. Gunawardena, G.; Hills, G.; Montenegro, I.; Scharifker, B. *J. Electroanal. Chem.* **1982**, *138*, 225.
28. Alvarez, A. E.; Salinas, D. R. *Electrochim. Acta* **2010**, *55*, 3714.
29. Lee, J. J.; Miller, B.; Shi, X.; Kalish, R.; Wheeler, K. A. *J. Electrochem. Soc.* **2001**, *148*, C183.
30. Palomar-Pardave, M.; Ramirez, M. T.; Gonzalez, I.; Serruya, A.; Scharifker, B. R. *J. Electrochem. Soc.* **1996**, *143*, 1551.
31. Heerman, L.; Tarallo, A. *J. Electroanal. Chem.* **1999**, *470*, 70.
32. Scharifker, B. R.; Mostany, J. *J. Electroanal. Chem.* **1984**, *177*, 13.
33. Sluyters-Rehbach, M.; Wijenber, J. H. O. J.; Bosco, E.; Sluyters, J. H. *J. Electroanal. Chem.* **1987**, *236*, 1.
34. Heerman, L.; Tarallo, A. *J. Electroanal. Chem.* **1998**, *451*, 101.
35. Deutscher, R. L.; Fletcher, S. *J. Electroanal. Chem.* **1988**, *239*, 17.